NANO LETTERS

Letter

pubs.acs.org/NanoLett

Multiband Hot Photoluminescence from Nanocavity-Embedded Silicon Nanowire Arrays with Tunable Wavelength

Zhiqiang Mu,[†] Haochi Yu,[‡] Miao Zhang,[†] Aimin Wu,[†] Gongmin Qi,[†] Paul K. Chu,[∥] Zhenghua An,[*,‡,§] Zengfeng Di,[*,†] and Xi Wang[†]

[†]State Key Laboratory of Functional Materials for Informatics, Shanghai Institute of Microsystem and Information Technology, Chinese Academy of Sciences, Shanghai 200050, People's Republic of China

[‡]State Key Laboratory of Surface Physics, Department of Physics and [§]Collaborative Innovation Center of Advanced Microstructures, Fudan University, Shanghai 200433, People's Republic of China

[∥]Department of Physics and Materials Science, City University of Hong Kong, Tat Chee Avenue, Kowloon, Hong Kong, People's Republic of China

S *Supporting Information*

ABSTRACT: Besides the well-known quantum confinement effect, hot luminescence from indirect bandgap Si provides a new and promising approach to realize monolithically integrated silicon optoelectronics due to phonon-assisted light emission. In this work, multiband hot photoluminescence is generated from Si nanowire arrays by introducing trapezoid-shaped nanocavities that support hybrid photonic-plasmonic modes. By continuously adjusting the geometric parameters of the Si nanowires with trapezoidal nanocavities, the multiband hot photoluminescence can be tuned in the range from visible to near-infrared independent of the excitation laser wavelength. The highly tunable wavelength bands and concomitant compatibility with Si-integrated electronics enable tailoring of silicon-based light sources suitable for next-generation optoelectronics devices.

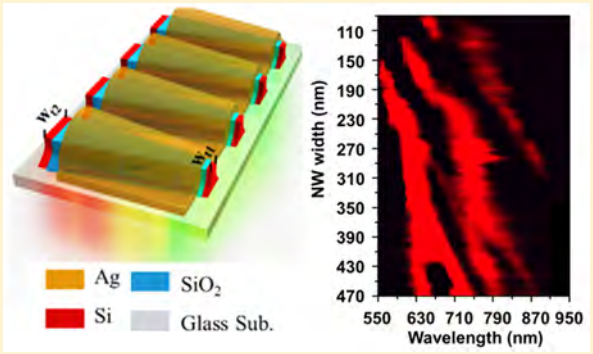

KEYWORDS: *Hot luminescence, Si nanowires, nanocavities, surface plasmon, resonance mode, tunable wavelength*

In the pursuit of higher performance, smaller power consumption, and lower cost per unit, Moore's law has been valid for complementary metal-oxide-semiconductor (CMOS) integrated circuit (IC) for decades.[1] However, on the heels of the increasing integration density and complexity of Si CMOS, there are severe challenges including signal propagation delay, heat dissipation, and limited bandwidth hindering the development of high-performance and low-power devices such as large-scale data centers and smartphones, and even much more advanced fin field-effect transistors (FinFETs) have joined.[2−4] Introduction of Si photonics to state-of-the-art ICs is regarded as a promising solution to achieve large bandwidths and low energy consumption.[5,6]

Although photonics-based modules such as photodetectors,[7] modulators,[8] and optical waveguides[9] have been developed using CMOS-compatible processes, the light sources are mainly based on III/V compound semiconductors instead of silicon because of the low emission efficiency of indirect bandgap Si.[10] Much effort has been made to overcome this limitation, for example, by introducing quantum confinement effects[11,12] or photonic crystals.[13,14] Unfortunately, most of these approaches are not practical, especially when considering monolithic integration into the exiting CMOS technology. For indirect bandgap semiconductors like Si, it is more challenging because phonons are involved in the light emission process and more complex radiative and nonradiative recombinations coexist and even compete,[15−17] resulting in low light emission efficiency. Taking advantage of the nanoplasmonic resonance and the associated huge Purcell enhancement (>1000),[18,19] recent breakthroughs on developing light sources for Si photonics have been demonstrated on direct bandgap CdS[19] and indirect-bandgap Si[20] by Cho et al. For indirect-bandgap Si material, when silicon nanowire is coupled with a Ω-shaped plasmonic cavity, the remarkable radiative rate enhancement of $>10^3$ with subpicosecond lifetimes and a spontaneous emission with the enhancement rate of 10^3 have been demonstrated. Despite the controversial luminescence mechanism,[21−23] this work undoubtedly assures the prominent merits of the phonon-assisted Si hot luminescence and suggests interesting physics among the three types of interacting species, namely charge, phonon, and cavity photon or plasmon. However, the proposed approach relies on randomly distributed silicon nanowires instead of

Received: November 8, 2016
Revised: January 10, 2017
Published: January 30, 2017

DOI: 10.1021/acs.nanolett.6b04675
Nano Lett. 2017, 17, 1552−1558

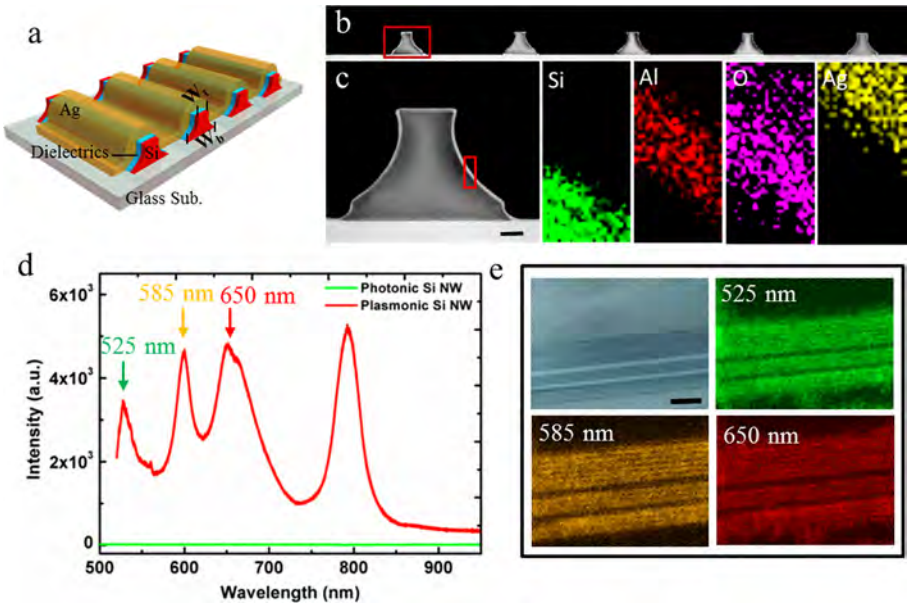

Figure 1. (a) Schematic of the trapezoidal nanocavity-embedded Si nanowire array. (b) Cross-sectional STEM image of nanocavities-embedded Si nanowire array. (c) Enlarged STEM image of a single nanocavity-embedded Si nanowire with SiO_2/Al_2O_3/Ag coating and EDS maps of Si, Al, O, and Ag of the nanocavity-embedded Si nanowire. The red rectangular area in the STEM image is selected for EDS mapping. Scale bar: 50 nm. (d) Room-temperature PL spectra of the Si nanowires with/without Ag-coated trapezoidal nanocavities. (e) Optical (upper left) and confocal laser fluorescence microscopy images of the Si nanowire array. The wavelength of excitation laser is 405 nm and the scale bar is 8 μm.

silicon nanowire array, which is commonly adopted by the state-of-the-art ICs, therefore, it is not a practical solution for silicon-based light source in term of CMOS compatibility. Meanwhile, as the optical modes corresponding to Si nanowires with fixed shape and dimension are limited, the wavelength tunability and the spectrum range of phonon-assisted Si hot luminescence are restricted as well, which cannot meet the broadband demand for optical communications of silicon photonics. Furthermore, as the luminescence mechanism for plasmonic nanocavity system is still unclear,[21−23] it is of fundamental importance to understand the more general light-matter interaction physics in indirect semiconductor embedding nanocavity systems.

In this work, trapezoidal nanocavities-embedded Si nanowire arrays with controllable dimension fabricated by CMOS process are investigated for phonon-assisted Si hot luminescence. The fabrication process is similar to that of trapezoidal-shaped FinFETs, which have been recently introduced to build 22 nm high-performance and low-power CMOS technology,[24] though the dimension of individual Si nanowire is enlarged for better visibility. Hot luminescence from trapezoidal Si nanowire is found to be governed by the plasmonic cavity mode with remarkably attenuated dependence on the intrinsic density of state of the phonon. By adjusting the geometric parameters of the Si nanowires via nanofabrication process, the multiband hot photoluminescence associated with different orders of cavity modes can be conveniently tuned in the range from visible to near-infrared. Meanwhile, inheriting the small mode volume of CMOS-compatible nanowire structures, the trapezoidal Si system preserves a large Purcell factor ($\sim 1 \times 10^2$) producing enhanced luminescence. The proposed Si light source with highly tunable wavelengths is promising to Si photonics as well as sensing and biomedical application.

The array of Si nanowires with the identical trapezoidal structure was fabricated on a silicon-on-insulator (SOI) wafer by electron beam lithography (EBL) and modified inductively coupled plasma (ICP) etching. After transferring to a quartz substrate by the sacrificial etching of the buried oxide, 5 nm Al_2O_3 layer and 120 nm Ag layer were deposited successively to produce the trapezoidal plasmonic nanocavity-coupled silicon nanowire device (see Supporting Information), as shown in Figure 1a,b. The plasmonic cavity was confined by the unique hornlike metal coverage and Si/quartz interface (with a refractive index ratio of about 3.42/1.46). Transmission electron microscopy (TEM), scanning transmission electron microscopy (STEM), and energy-dispersive X-ray spectroscopy (EDS) reveal that the dielectric layer consists of 3 nm native oxide and 5 nm Al_2O_3, as shown in Figure S1 and Figure 1c.

Room-temperature photoluminescence (PL) from a typical array of trapezoidal nanocavities embedded Si nanowires with top width W_t of 130 nm and bottom width W_b of 330 nm was monitored with a perpendicularly polarized 514 nm Ar laser. The laser spot size is ~700 nm and the corresponding power density is ~2.6 mW/μm^2. A broadband hot luminescence spectrum with considerable counts is observed, as shown in Figure 1d. In addition, four distinct peaks emerge from the broadband PL spectrum of the nanocavity-embedded Si nanowires. There are at least four resonant modes along the metal/dielectrics interface perpendicular to the long axis of the nanowires. In contrast, no appreciable counts above the background can be detected from the array of Si nanowires coated with the identical dielectric layers but without Ag nanocavities. The difference suggests that strong confinement from the plasmonic trapezoidal nanocavities is responsible for the broadband hot luminescence. To characterize the real emission color of the nanocavity-embedded Si nanowire array, confocal laser fluorescence microscopy images acquried with 40× objective and 405 nm laser at single detection channel are shown in Figure 1e. The spot size of 405 nm laser is ~520 nm, and the corresponding laser power density is ~17.9 mW/μm^2. The figure in the upper left panel is the optical image of the array consisting of 12 individual Si nanowires and the other

DOI: 10.1021/acs.nanolett.6b04675
Nano Lett. 2017, 17, 1552−1558

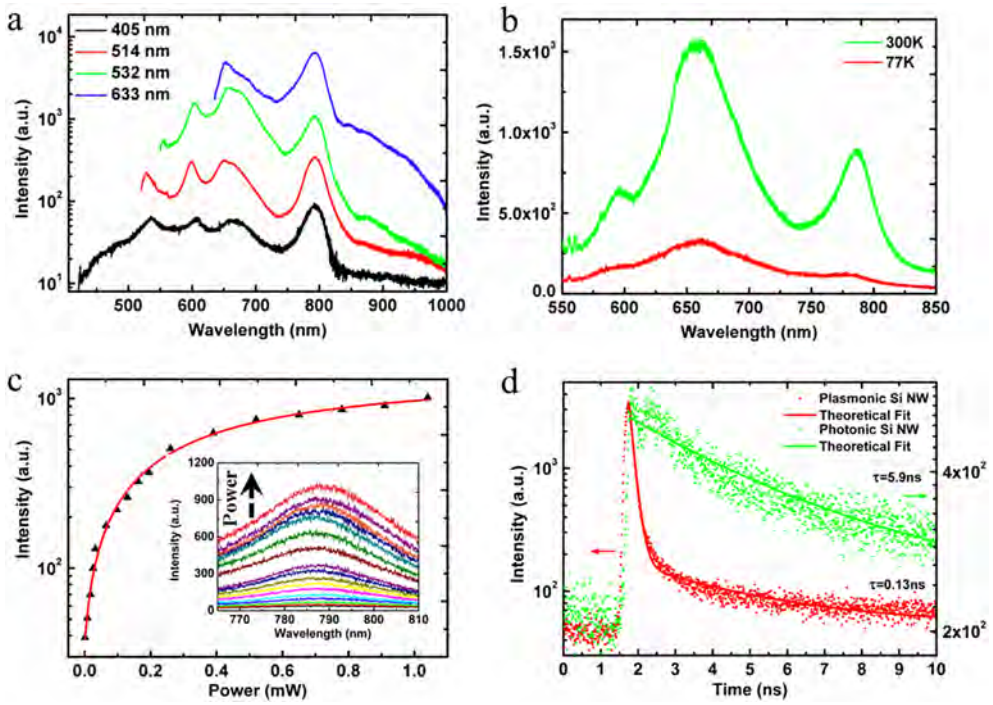

Figure 2. (a) Room-temperature PL spectra of the trapezoidal nanocavity-embedded Si nanowire array excited by 405, 514, 532, and 633 nm laser lines. Each spectral curve has been normalized and offset for clarity purpose. (b) PL spectra of the trapezoidal nanocavity-embedded Si nanowire array at 77 and 300 K. (c) Room-temperature PL intensity of the trapezoidal nanocavity-embedded Si nanowire array as a function of excitation power. The inset shows the corresponding PL spectra with different excitation power of the 514 nm laser. (d) Time-resolved hot luminescence decay of the plasmonic Si nanowire (with Ag coating) and the photonic Si nanowire (without Ag coating) at room temperature. The emission lifetime is extracted from the exponential fitting curve.

three figures are the corresponding confocal laser fluorescence images obtained using 525, 585, and 650 nm channels, respectively. Three fluorescence images also show the alignment of silicon nanowires but three different colors of green, yellow, and red, which are consistent with three strong hot luminescence bands in the visible region, as shown in Figure 1d. In addition, the fouth strong hot luminescence band at 793 nm, which is located in the near-infrared region, cannot be resolved by confocal laser fluorescence microscopy. Other than the silicon nanowire array, the more complex pattern "SIMIT" (abbreviation of our institute) composed of silicon nanowires can be fabricated (Figure S2) and each letter shows broadband hot luminescence. The letter "SIMIT" can be selectively displayed by PL mapping of the luminescence peak, for example, at 650 and 750 nm.

Room-temperature PL is monitored with four different laser lines of 405, 514, 532, and 633 nm to characterize the nanocavity-embedded Si nanowires. As shown in Figure 2a, the peak positions are always fixed irrespective of the energy of the excitation laser. It is similar to the usual light emission of near-band-edge combination but different from that observed from Ω-shaped cavities.[21] This implies that in the trapezoidal Si nanowires, radiative recombination of excited carriers occurs at the resonance frequencies of the cavity modes involving real electronic states (not necessarily to be band minima such as X, L in electronic band diagram). In contrast, involvement of the real or virtual electronic states has to be precautiously justified in Ω-cavities in order to be distinguished from resonant Raman process.[23] The cavity modes for a particular nanowire are spectrally fixed by its geometry and the tunability of hot luminescence from the trapezoidal cavity embedded Si nanowires can be inferred. For different batches of nanowires with the same size, the luminescence bands are always independent of the laser excitation energy and it is rather important to attain tunable luminescence by engineering the cavity resonances later.

To investigate the origin of hot luminescence, the nanocavity-embedded Si nanowire array is studied by monitoring the PL spectra at different temperatures, as shown in Figure 2b. The photoluminescence intensity is enhanced as the measurement temperature is increased from 77 to 300 K and the integrated intensity in the PL spectrum at 300 K is 5−10 times larger than that in the 77 K one. Therefore, the hot luminescence of nanocavity-embedded Si nanowire array exhibits a positive temperature dependence, which is contrary to that of direct bandgap materials like AlGaAs[25] and CdS.[26] The photoluminescence from direct bandgap materials is always suppressed at elevated temperature due to increased nonradiative recombination.[27] However, the process for hot luminescence from an indirect bandgap material (Si in trapezoidal cavities) is quite different, where the thermally activated phonons are necessary to mediate radiative recombination and satisfy momentum conservation. As the phonon population increases with temperature,[28] the hot luminescence from the nanocavity-embedded Si nanowire array is enhanced at elevated temperature accordingly. Previously, the similar positive temperature dependence of photoluminescence behavior has been observed in Ω-shaped plasmonically coupled Si nanowires[21,23] in which phonon mediated radiative recombination dominates. It is worth mentioning that the enhanced absorption coefficient of silicon at elevated temperature may also contribute to the increased PL intensity to some extent (~2.4 fold at most) but should not be the dominating reason as determined by the more quantitative analysis.[21]

DOI: 10.1021/acs.nanolett.6b04675
Nano Lett. 2017, 17, 1552−1558

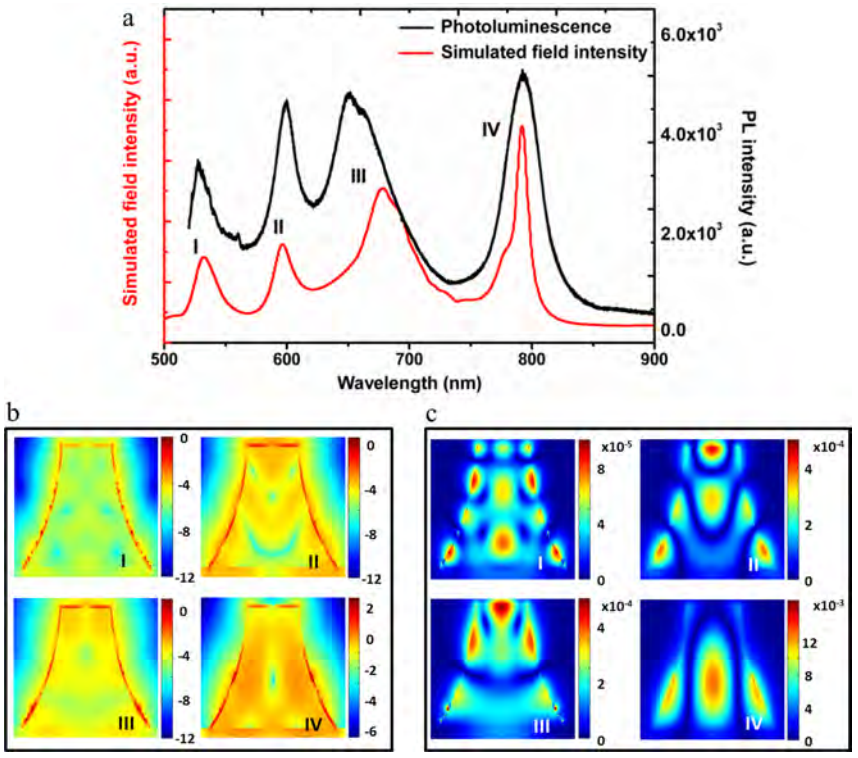

Figure 3. (a) Calculated frequency-dependent electromagnetic field intensity inside the nanocavity of the trapezoidal Si nanowire with the experimental PL spectrum included for comparsion. The four resonance modes labeled as I, II, III, and IV are observed. (b,c) The calculated electric and magnetic field profiles for resonance modes I, II, III, and IV, respectively.

The change in the PL intensity with excitation power is always investigated to study the recombination process for above-band gap excitation, especially for II–VI and III–V compound direct bandgap semiconductors.[29−31] The power dependence of the PL intensity can be described by an $I \sim P^{\alpha}$ law, where I is the luminescence intensity, P is the excitation laser power, and α is a dimensionless exponent.[29−31] With regard to the free- and bound-exciton emission, α is generally between 1 and 2 but is usually less than 1 for free to bound and donor–acceptor pair recombination. The PL spectra are acquired using a 514 nm laser with different excitation power at room temperature. The PL intensity at around 790 nm increases with excitation power as shown in the inset in Figure 2c. It follows a similar trend as the aforementioned direct bandgap semiconductors with α of ∼0.6. The sublinearity of the luminescence intensity with increasing pump power may be caused by the dynamic equilibrium between hot carrier radiation and intraband relaxation. The similarity of the trapezoidal Si ($\alpha \sim 0.6$) with free-to-bound and donor–acceptor pair recombination in direct bandgap semiconductors ($\alpha < 1$) suggests that the hot luminescent process is complex involving phonons. The reported $I \sim P^{\alpha}$ law is generally applied to direct bandgap semiconductor but it is noted that the comprehensive theory is still absent and has to be developed in the future to describe the nonlinear power dependence of hot carrier luminescence from nanocavity-embedded Si nanowires. The interactions among three particle systems (carriers, phonons, and cavity plasmons) and other nonlinear process (phonon intraband relaxation and Auger recombination) must be taken into account.

To confirm the radiative recombination enhancement, the time-resolved hot luminescence decay of cavity-embedded Si nanowires is monitored using time-correlated single photon counting (TCSPC) system in the emission range between 630 and 730 nm at pulsed excitation of λ_{ex} = 405 nm (Figure 2d). TCSPC system is extremely sensitive for weak emission, and it can even detect the spontaneous emission from photonic Si NWs without plasmonic nanocavity although it requires sufficiently long time to achieve reasonable photon counts. The light emission for plasmonic Si nanowires, that is, trapezoidal nanocavity-embedded Si nanowires with Ag coating exhibits an exponential decay with a spontaneous emission lifetime of ∼130 ps. It is reduced by a factor of 45 in comparison with photonic Si nanowires, that is, trapezoidal Si nanowires without Ag coating (∼5.9 ns). The lifetime appears to be very short compared to previous reports on indirect bandgap Si systems[28] but comparable to direct bandgap semiconductors such as the hybrid CdS–MgF_2–Ag nanosquares (∼72 ps).[32] The large radiative rate enhancement is believed to be caused by the ultrasmall mode volumes and reasonably high quality factors of the nanocavities that provide high electromagnetic energy densities.

To further investigate the enhanced electromagnetic field intensity in the cavity-embedded Si nanowire, finite-difference time-domain (FDTD) simulation is performed. The simulated frequency-dependent electromagnetic field intensity inside the nanocavity is enhanced at 532, 596, 677, and 792 nm (Figure 3a), indicating four resonance modes (I–IV) produced by the nanocavity. These peaks match well with four hot luminescence peaks obtained by the experimental PL results. The agreement between the simulation results and the experimental data suggests that radiative recombination of excited carriers occurs mainly at the resonance frequency of the cavity modes, suggesting that it is feasible to tailor the luminescent wavelengths by changing the dimensions of the cavities. As expected, the calculated electric and magnetic field profiles of

DOI: 10.1021/acs.nanolett.6b04675
Nano Lett. 2017, 17, 1552–1558

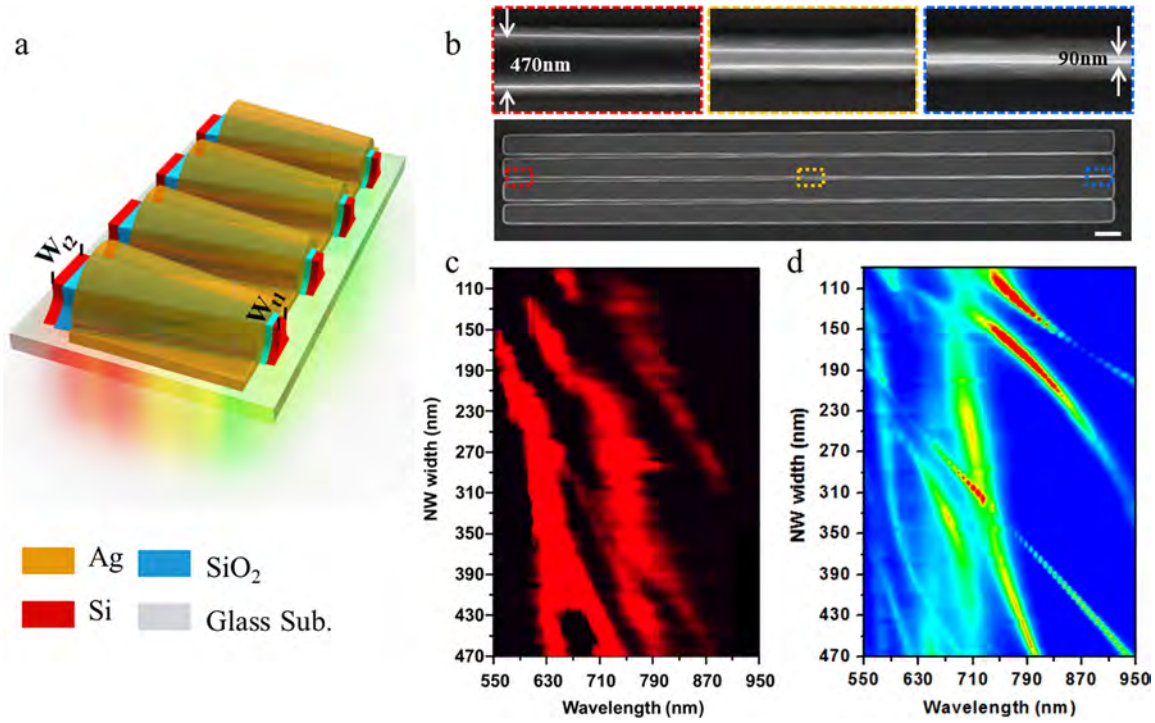

Figure 4. (a) Schemetic of hot luminescence with variable wavelengths from the trapezoidal nanocavity-embedded Si nanowire array with continuously varying sizes. (b) SEM images of the Si nanowire array with W_t ranging from 470 to 90 nm. Scale bar: 2 μm. (c) Normalized PL spectra of the trapezoidal nanocavity-embedded Si nanowires with W_t ranging from 470 to 90 nm. (d) Calculated field intensity spectra of the trapezoidal nanocavity-embedded Si nanowires with continuously varying widths measured in (c).

the four resonant cavity modes (I–IV) show that the electromagnetic field is not only confined in the gap region between the metal surface and Si nanowires, but also more importantly inside the Si nanowires (Figure 3b,c) thus enhancing the light-matter (Si) interaction. The resonant modes verify that the confinement by the Ag and Si/quartz interface is sufficient even though the Si/quartz interface allows moderate transmission. The electromagnetic field of a pure surface plasmon state is confined to the metal surface with exponentially decaying profiles away from the metal sufarce and so there is large metallic ohmic loss. In our trapezoidal nanocavities, however, the plasmonic resonant modes are hybridized with photonic ones and a significant portion of the electromagnetic field is located inside the nanowire to contribute to the light-matter (Si) interaction. Because the electric field is preferentially perpendiular to the long axis of the nanowire in the hybrid plasmonic modes, the parallel polarized PL intensity is suppressed giving rise to the obvious polarization dependence on emission polarization (Figure S3). For comparison, the polarization dependence of excitation polarization shows no clear difference, and experiments (Figure S4) under parallel (photonic-like) and perpendicular (plasmonic-like) excitations show comparable luminescent intensities, which agrees well with earlier work with large size nanowire.[21] The experimental observation is also consistent with our theoretical simulations that predicts comparable Si absorption efficiencies under parallel/perpendicular laser excitations at 514 nm (not shown). Because the hot luminescence from Si is an inelastic and incoherent process, the PL signal becomes nearly independent of the excitation polarization once the excitation energy is absorbed by the embedded Si. Consequently, the PL intensity is justified by the Purcell enhancement effect[21] that prefers the plasmonic-like modes and therefore perpendicular emission polarization. The stronger dependence of hot luminescence on emission polarization rather than excitation polarization suggests that the optical cavity modes in lieu of the intrinsic density of phonon state play a crucial role in the hot luminescent emission from the trapezoidal samples.

The spontaneous emission rate enhancement of a dipole source observed by Purcell[33] is given by

$$F_p = \frac{\gamma}{\gamma_0} = \frac{3}{4\pi^2}\left(\frac{\lambda_c}{n}\right)^3\left(\frac{Q}{V_m}\right)$$

where γ and γ_0 are the spontanous emssion rates in the host medium and free space, respectively, and λ_c, n, Q, and V_m are the vacuum wavelength, refractive index, quality factor, and mode volume, respectively.[17,34] The spontaneous emission rate enhancement known as the Purcell effect is determined by Q and V_m. As the optical cavity has entered into nanoscale, the quality factor of the cavity mode Q is reduced slightly (less than 10^2) compared to the microscale counterpart. However, the mode volume V_m shrinks more dramatically, thus resulting in a larger F_p. Therefore, enhanced spontaneous emission can be achieved from the ultrasmall optical cavity. The quality factor Q of the hybrid cavity mode is estimated to be ~60 with the frequency at around 792 nm (mode IV in Figure 3a) and mode volume of $\lambda_c^3/10^3$ (λ_c is the free-space wavelength).[35] It leads to a Purcell factor of $\sim 1 \times 10^2$, which is the same magnitude as that reported by Mokkapati et al.[35]

The luminescence property of the trapezoidal nanocavity embedded Si nanowires is determined by the cavity modes instead of the intrinsic phonon band structure. Therefore, the luminescence band of the nanocavity-embedded Si nanowires can be easily tuned by changing the dimensions of the Si

DOI: 10.1021/acs.nanolett.6b04675
Nano Lett. 2017, 17, 1552–1558

nanowires. When the size of the nanocavity is changed continuously, the nanocavity resonance modes are expected to shift gradually, as schematically illustrated in Figure 4a. As a result of the precise CMOS nanofabrication process, Ag/SiO_2 layer-coated Si trapezoidal nanocavity arrays with continuously varying widths between 90 and 470 nm are fabricated (Figure 4b). The normalized PL spectra (Figure 4c and Figure S5) show that the luminescence bands shift to lower wavelength (blue shift) as the top width of the trapezoidal nanocavity W_t decreases. In particular, as W_t is changed from 470 to 90 nm, the three typical luminsecent peaks shift from ~750 to ~550 nm, ~870 to ~630 nm, and ~900 to ~670 nm, corresponding to the tunability ratios of about 31%, 32%, and 29%, respectively. Moreover, four distinct emission peaks emerge from the nanocavities with large W_t (430 nm < W_t < 470 nm). As the top width of the trapezoidal nanocavity W_t is decreased, the two emission peaks at lower wavelengths (630−750 nm) merge into a single peak, while the other two emission peaks at higher wavelengths (790−880 nm) merges first and then splits. The luminescence band evolution is also revealed by numerical simulation of the field intensity as a function of nanowire size, as shown in Figure 4d. Considering the dispersive refractive index of Si in this wide wavelength range and also imperfection in nanofabrication, the agreement between the simulation (Figure 4d) and experimental data (Figure 4c) is quite good. In addition, the polarization-dependent data (Figure S6) show consistency with the cavity mode simulation, which further proves that wavelength tuning indeed originates from the cavity modes, because the electronic band and phonon density of states are both fixed in the gradient nanowires. Most of the luminescent range (600−950 nm) in Figure 4c is below the L-point bandgap but still above the X-point bandgap and the luminescence thus arises from hot electrons along the Γ−X electronic branch and no peak emission is shown without regulation by the photon or phonon density of states. In practice, the trapezoidal cavity resonances (Figure 4d) show up in the same wavelength range and exhibit a similar blue shift tendency with decreasing cavity size, producing evidence that photon rather than phonon density of states plays a crucial role here.

As shown by the experimental and simulation results in Figure 4, the luminescence bands of the Si nanowires with trapezoidal nanocavities can be tuned by the cavity resonance modes. Thus, the wavelength of the emission peaks can be simply tuned by designing the Si nanowires with particular dimensions. For a Ω-shaped cavity, the plasmonic cavity modes can also be adjusted by changing the diameter of the Si nanowires. Nevertheless, the strong hot luminescence bands of Si nanowires are fixed at around 2.51, 2.34, and 2.18 eV without any shift when perfect matching is satisfied between cavity resonances and phonons with the largest density of states.[20,21] In the trapezoidal nanocavities, hot electrons emitted at a longer wavelength range (600−950 nm) exhibit larger momentum mismatch and therefore require participation of multiple phonons. Because of the multiple-phonon involvement and many possible pathways, the spectral features modulated by specific phonon with high density of states becomes less noticeable and the spectral tunability by cavity modes becomes prominent compared to Ω-shaped cavity.[20,21] Furthermore, when the nanowire is optically excited, electrons may be excited with higher efficiency. The hot phonon population and subsequent phonon bottleneck of carrier relaxation may emerge. It is believed that nonequilibrium distributed phonons produced by hot carriers can be reabsorbed by the relaxing charge carriers to retard the charge carriers relaxation process. As the time for radiative recombination is sufficiently shortened by the cavity modes, the dependence of the intrinsic phonons with a large density of states will be reduced, as suggested by the weaker temperature dependence of hot luminescence.[36−38] Our work together with existing works reveals the rich physics of hot electron relaxation dynamics interacting with other (quasi-)particles such as phonon and cavity-photon/plasmon, and the realized tunable emission in this work implies the new possibility to engineer the luminescent property of indirect semiconductor with the advanced nanotechnology.

In conclusion, we demonstrate large enhancement in the hot luminescence from Si nanowire arrays embedded with trapezoidal nanocavities fabricated by CMOS-compatible processes. The luminescence from trapezoidal nanocavity-embedded Si nanowire arrays has unique properties including a very short radiative lifetime (~130 ps), positive temperature dependence, power law dependence on excitation laser power ($I \sim P^{\alpha}$, with $\alpha \sim 0.6$), and most importantly, wide wavelength tunability with cavity resonance, which is in contrast to the phonon-dominated Ω-shaped Si nanowire case. The independence of the hot luminescence bands with excitation laser shows that hot carrier radiation recombination in the trapezoidal cavity-embedded Si nanowires is not restricted by the intrinsic phonon density of states. The hot luminescence bands can be conveniently tuned via cavity resonance modes by simply dimension adjustment of Si nanowires. The excellent wavelength tunability of trapezoidal Si nanowire system is expected to promote its potential for future Si photonics, sensing, and biomedical research applications.

■ ASSOCIATED CONTENT

Supporting Information

The Supporting Information is available free of charge on the ACS Publications website at DOI: 10.1021/acs.nanolett.6b04675.

Experimental methods, luminescence spectra images and FDTD simulation results (PDF)

■ AUTHOR INFORMATION

Corresponding Authors

*E-mail: anzhenghua@fudan.edu.cn.
*E-mail: zfdi@mail.sim.ac.cn.

ORCID

Zengfeng Di: 0000-0002-9357-5107

Author Contributions

Z.D. and X.W. supervised the project. Z.D., M.Z., Z.A., and Z.M. conceived and designed the experiments. Z.D. and Z.M. fabricated the samples and carried out experimental measurements. H.Y., G.Q., and Z.A. performed the FDTD simulation. Z.D., Z.A., A.W., P.K.C., Z.M., and H.Y. analyzed the data and cowrote the paper. All the authors discussed the results and commented on the manuscript. Z.M. and H.Y. contributed equally to this work.

Notes

The authors declare no competing financial interest.

■ ACKNOWLEDGMENTS

The authors thank the financial support from National Natural Science Foundation of China (61274136/11427807/

DOI: 10.1021/acs.nanolett.6b04675
Nano Lett. 2017, 17, 1552−1558

11634012/11674070), Creative Research Groups of National Natural Science Foundation of China (No. 61321492), Program of Shanghai Academic/Technology Research Leader (16XD1404200), and City University of Hong Kong Applied Research Grant (ARG) 9667122.

REFERENCES

(1) Chau, R.; Doyle, B.; Datta, S.; Kavalieros, J.; Zhang, K. *Nat. Mater.* **2007**, *6*, 810−812.
(2) del Alamo, J. A. *Nature* **2011**, *479*, 317−323.
(3) Frank, D. J. *IBM J. Res. Dev.* **2002**, *46*, 235−244.
(4) Theis, T. N.; Solomon, P. M. *Proceedings of the IEEE 2004 International Interconnect Technology Conference* **2010**, *98*, 2005−2014.
(5) Chen, X.; Li, C.; Tsang, H. K. *NPG Asia Mater.* **2011**, *3*, 34−40.
(6) Sun, C.; Wade, M. T.; Lee, Y.; Orcutt, J. S.; Alloatti, L.; Georgas, M. S.; Waterman, A. S.; Shainline, J. M.; Avizienis, R. R.; Lin, S.; Moss, B. R.; Kumar, R.; Pavanello, F.; Atabaki, A. H.; Cook, H. M.; Ou, A. J.; Leu, J. C.; Chen, Y. H.; Asanovic, K.; Ram, R. J.; Popovic, M. A.; Stojanovic, V. M. *Nature* **2015**, *528*, 534−538.
(7) Assefa, S.; Xia, F. N. A.; Vlasov, Y. A. *Nature* **2010**, *464*, 80−84.
(8) Xu, Q. F.; Schmidt, B.; Pradhan, S.; Lipson, M. *Nature* **2005**, *435*, 325−327.
(9) Xia, F. N.; Sekaric, L.; Vlasov, Y. *Nat. Photonics* **2007**, *1*, 65−71.
(10) Liu, J. F.; Camacho-Aguilera, R.; Bessette, J. T.; Sun, X. C.; Wang, X. X.; Cai, Y.; Kimerling, L. C.; Michel, J. *Thin Solid Films* **2012**, *520*, 3354−3360.
(11) Cullis, A. G.; Canham, L. T. *Nature* **1991**, *353*, 335−338.
(12) Wilson, W. L.; Szajowski, P. F.; Brus, L. E. *Science* **1993**, *262*, 1242−1244.
(13) Akahane, Y.; Asano, T.; Song, B. S.; Noda, S. *Nature* **2003**, *425*, 944−947.
(14) Fujita, M.; Takahashi, S.; Tanaka, Y.; Asano, T.; Noda, S. *Science* **2005**, *308*, 1296−1298.
(15) Goldman, J. R.; Prybyla, J. A. *Phys. Rev. Lett.* **1994**, *72*, 1364−1367.
(16) Liang, D.; Bowers, J. E. *Nat. Photonics* **2010**, *4*, 511−517.
(17) Aspetti, C. O.; Agarwal, R. *J. Phys. Chem. Lett.* **2014**, *5*, 3768−3780.
(18) Bergman, D. J.; Stockman, M. I. *Phys. Rev. Lett.* **2003**, *90*, 027402.
(19) Cho, C. H.; Aspetti, C. O.; Turk, M. E.; Kikkawa, J. M.; Nam, S. W.; Agarwal, R. *Nat. Mater.* **2011**, *10*, 669−675.
(20) Cho, C. H.; Aspetti, C. O.; Park, J.; Agarwal, R. *Nat. Photonics* **2013**, *7*, 285−289.
(21) Aspetti, C. O.; Cho, C. H.; Agarwal, R.; Agarwal, R. *Nano Lett.* **2014**, *14*, 5413−5422.
(22) Russell, K. J.; Hu, E. L. *Nat. Photonics* **2014**, *8*, 666−666.
(23) Aspetti, C. O.; Cho, C. H.; Park, J.; Agarwal, R. *Nat. Photonics* **2014**, *8*, 667−668.
(24) Intel Corporation. *3-D, 22nm: New TechnologyDelivers An Unprecedented Combination ofPerformance and Power Efficiency*. www.intel.com/content/www/us/en/silicon-innovations/intel-22nm-technology.html.
(25) Titova, L. V.; Hoang, T. B.; Jackson, H. E.; Smith, L. M.; Yarrison-Rice, J. M.; Kim, Y.; Joyce, H. J.; Tan, H. H.; Jagadish, C. *Appl. Phys. Lett.* **2006**, *89*, 173126.
(26) Hoang, T. B.; Titova, L. V.; Jackson, H. E.; Smith, L. M.; Yarrison-Rice, J. M.; Lensch, J. L.; Lauhon, L. J. *Appl. Phys. Lett.* **2006**, *89*, 123123.
(27) Pankove, J. I. *Optical processes in semiconductors*; Prentice-Hall: Englewood Cliffs, NJ, 1971.
(28) Kwack, H. S.; Sun, Y.; Cho, Y. H.; Park, N. M.; Park, S. J. *Appl. Phys. Lett.* **2003**, *83*, 2901−2903.
(29) Cooper, D. E.; Bajaj, J.; Newman, P. R. *J. Cryst. Growth* **1988**, *86*, 544−551.
(30) Schmidt, T.; Lischka, K.; Zulehner, W. *Phys. Rev. B: Condens. Matter Mater. Phys.* **1992**, *45*, 8989−8994.
(31) Daoudi, M.; Kaouach, H.; Dhifallah, I.; Ouerghi, A.; Chtourou, R. *Optik* **2015**, *126*, 932−936.
(32) Ma, R. M.; Oulton, R. F.; Sorger, V. J.; Bartal, G.; Zhang, X. *Nat. Mater.* **2011**, *10*, 110−113.
(33) Purcell, E. M. *Phys. Rev.* **1946**, *69*, 37.
(34) Piccione, B.; Aspetti, C. O.; Cho, C. H.; Agarwal, R. *Rep. Prog. Phys.* **2014**, *77*, 086401.
(35) Mokkapati, S.; Saxena, D.; Jiang, N.; Li, L.; Tan, H. H.; Jagadish, C. *Nano Lett.* **2015**, *15*, 307−312.
(36) Nozik, A. J. *Annu. Rev. Phys. Chem.* **2001**, *52*, 193−231.
(37) Tea, E.; Hamzeh, H.; Aniel, F. *J. Appl. Phys.* **2011**, *110*, 113108.
(38) Conibeer, G.; Patterson, R.; Huang, L. M.; Guillernoles, J. F.; Konig, D.; Shrestha, S.; Green, M. A. *Sol. Energy Mater. Sol. Cells* **2010**, *94*, 1516−1521.

DOI: 10.1021/acs.nanolett.6b04675
Nano Lett. 2017, 17, 1552−1558

Supporting Information for

Multiband Hot Photoluminescence from Nanocavity-Embedded Silicon Nanowire Arrays with Tunable Wavelength

Zhiqiang Mu[†], Haochi Yu[‡], Miao Zhang[†], Aiming Wu[†], Gongmin Qi[†], Paul K. Chu[‖], Zhenghua An[*,‡,§], Zengfeng Di[*,†], Xi Wang[†]

[†] State Key Laboratory of Functional Materials for Informatics, Shanghai Institute of Microsystem and Information Technology, Chinese Academy of Sciences, Shanghai 200050, People's Republic of China

[‡] State Key Laboratory of Surface Physics, Department of Physics and [§] Collaborative Innovation Center of Advanced Microstructures, Fudan University, Shanghai 200433, People's Republic of China

[‖] Department of Physics and Materials Science, City University of Hong Kong, Tat Chee Avenue, Kowloon, Hong Kong, People's Republic of China

Methods

Device fabrication and characterization

The 25 μm long Si nanowire array was fabricated on an undoped SOI substrate with a top Si layer of 190 nm and buried oxide (BOX) of 145 nm by electron beam lithography (EBL) and inductively coupled plasma (ICP) etching. The trapezoidal structure was formed purposely during ICP by using SF_6 gas but without CF_4 passivation gas. The top width of Si nanowire with the trapezoidal structure was controlled precisely by the lithographic process. After etching the undernearth BOX layer using HF solution, the Si nanowire array was transferred to a 50 μm-thick quartz substrate. A 5 nm Al_2O_3 dielectric layer was deposited by atomic layer deposition (ALD) (Beneq TFS 200) at 200 ^oC using trimethyl aluminum ($Al(CH_3)_3$) as the metal precursor and O_2 as the oxidant after the growth of 3 nm native oxide on the nanowire, which was used as a blocking layer to reduce propagation loss from the metal while maximizing the nanocavity electromagnetic fields at the interface. Finally, 120 nm Ag was deposited by magnetron sputtering at the rate of 0.6Å/s at room temperature to form the plasmonic Si nanowire array. The Si nanowire array without Ag deposition (photonic Si nanowire array) was prepared for comparison. The whole structure of plasmonic Si nanowire, i.e., trapezoidal nanocavitie-embedded Si nanowire with Ag coating is revealed by transmission electron microscopy (TEM), as shown in Figure S1. For Si trapezoidal nanocavity arrays with continuously varying widths shown in Figure 4, only 3 nm native oxide was used as a blocking layer

between Si nanowire and Ag coating to reduce propagation loss from the metal while maximizing the nanocavity electromagnetic fields at the interface.

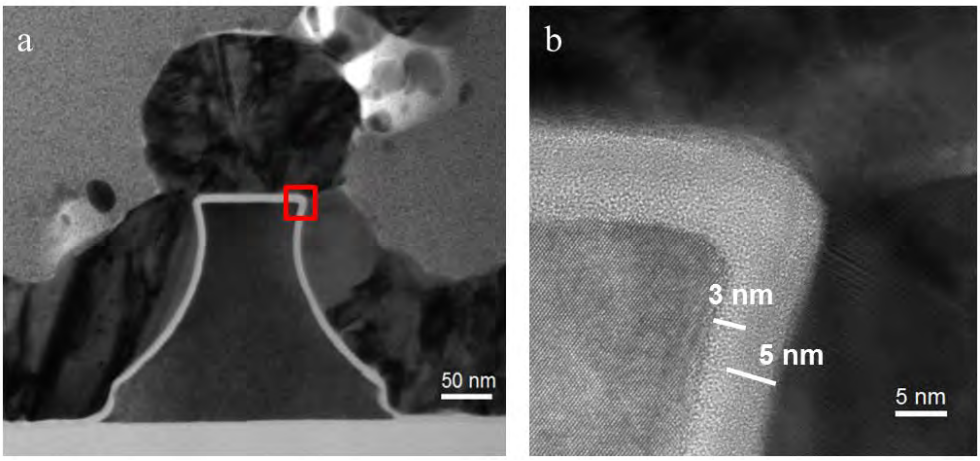

Figure S1. (a) TEM image of trapezoidal nanocavitie-embedded Si nanowire with Ag coating. Trapezoidal shaped Si nanowire is coated with dielectric layer and polycrystalline Ag layer. (b) High resolution TEM image reveals that the dielectric layer consists of 3 nm native oxide and 5 nm Al_2O_3 dielectric layer.

The photoluminescence spectra (PL) of the nanocavity-embedded Si nanowires were excited and collected through the transparent quartz substrate by confocal μ-Raman spectroscopy (HORIBA Jobin Yvon HR800) with the laser spot size less than 1 μm.

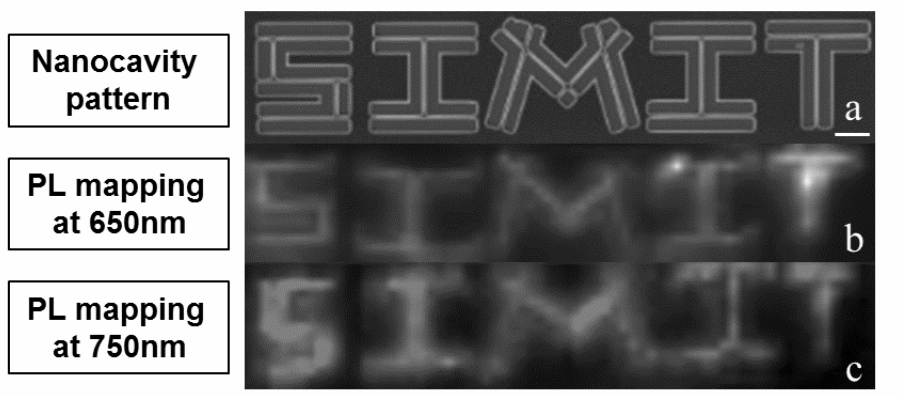

Figure S2. (a) SEM image of Si nanowires arranged as the letter "SIMIT". The scale bar is 2 μm. The PL maps of the trapezoidal nanocavity-embedded Si nanowires at luminescence peak at 650 nm (b) and 750 nm (c) at a scanning step of 0.5 μm.

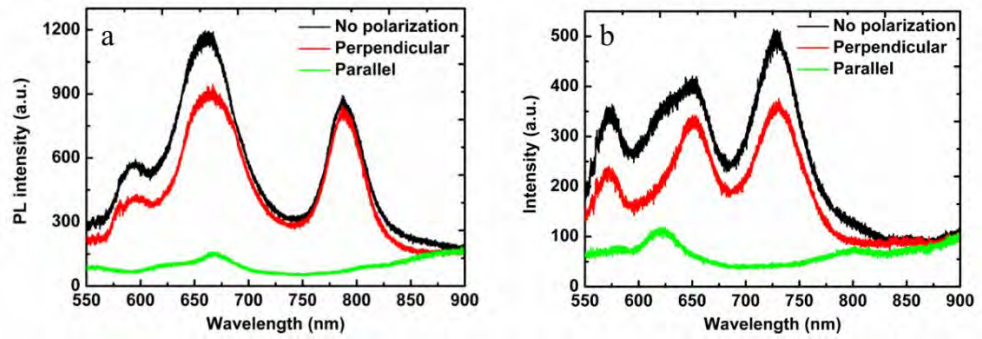

Figure S3. Polarization-resolved hot luminescence spectra of the trapezoidal nanocavities embedded Si nanowires for emission polarization in the Si nanowires of (a) W_t of 130 nm and W_b of 330 nm and (b) W_t of 90 nm and W_b of 290 nm. The parallelly polarized PL intensity is suppressed compared to the perpendicularly polarized PL, indicating strong mudualtion of the cavity modes in the hot luminesence process in the trapezoidal Si nanowires.

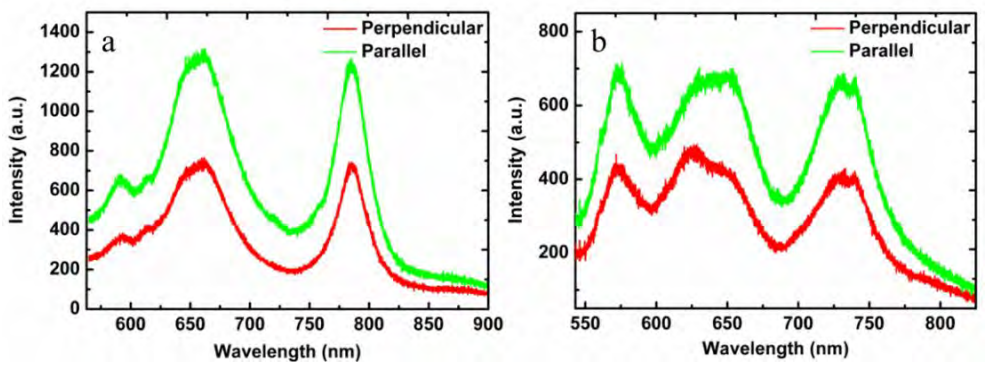

Figure S4. Hot photoluminescence spectra of the trapezoidal nanocavities embedded Si nanowires under different excitation polarization for samples with (a) W_t of 130 nm and W_b of 330 nm and (b) W_t of 90 nm and W_b of 290 nm. The main spectral features are identical for different excitation polarizations except the different background. Although the polarization ratio is relatively small, the coupling efficiency of parallel-polarized light to the long axis of trapezoidal naowires is higher than that perpendicularly polarized.

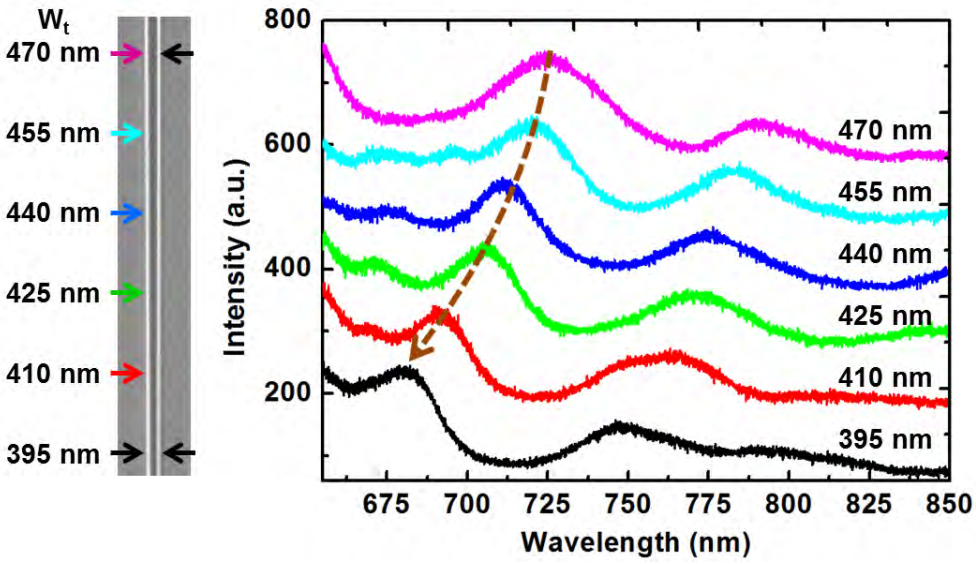

Figure S5. PL spectra of the trapezoidal nanocavities embedded Si nanowires with continuously changing width from 470 nm to 395 nm. The typical hot luminescence bands of Si nanowires exhibits a blue shift from ~725 nm to ~680 nm. It is shown experimentally that the luminescence bands of the Si nanowires with trapezoidal nanocavities can be tuned by the cavity resonance modes. Hence, the wavelength of the emission peaks can be tuned by designing the Si nanowires with particular dimensions.

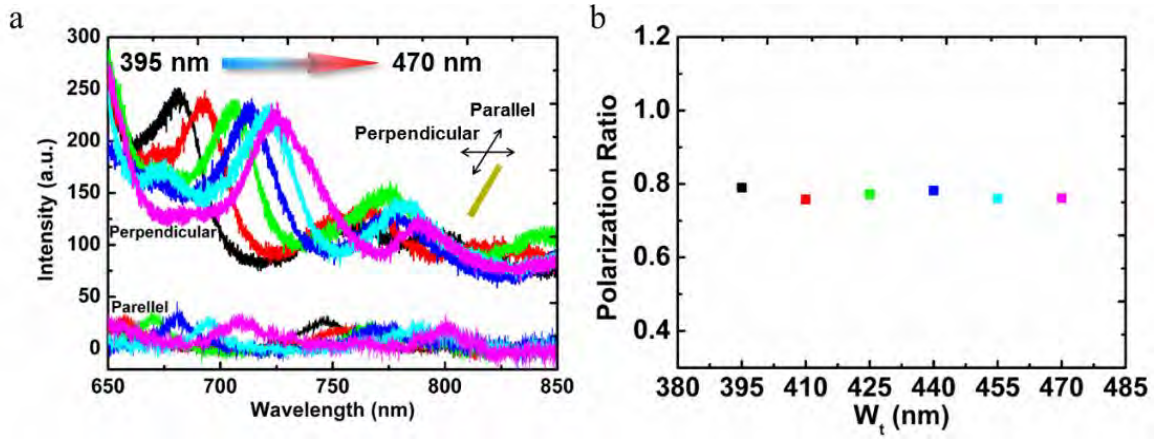

Figure S6. (a) Polarization-dependent PL spectra of the trapezoidal nanocavities embedded Si nanowires with continuouly changing widths (395 nm < W_t < 470 nm) as shown in Fig. S5. (b) Corresponding polarization ratio. The relatively large emission polarization ratio of about 0.77 confirms that the luminescence bands of the Si nanowires with trapezoidal nanocavities can be tuned by the cavity resonance modes.